

Variational calculation of polarization of quantum-well photoluminescence

A. Twardowski

Institute of Experimental Physics, The University of Warsaw, Hoza 69, PL-00-681 Warsaw, Poland

C. Hermann

Laboratoire de Physique de la Matière Condensée, Ecole Polytechnique, 91128 Palaiseau, France

(Received 5 January 1987)

We calculate for the first time the circular polarization of GaAs/Ga_{1-x}Al_xAs quantum-well photoluminescence taking into account the true nonparabolic valence-band structure. Versus the excitation energy, we find high positive polarization for the transition $n=1$ heavy-hole-to-conduction-band transition and negative polarization at the onset of $n=1$ light-hole-to-conduction-band transition in qualitative agreement with experiments. We also study the Ga_yIn_{1-y}As/InP system and predict no negative polarization in this case.

INTRODUCTION

The optical properties of GaAs/Ga_{1-x}Al_xAs quantum wells (QW's) have been widely studied, mostly by luminescence.¹ This technique allows one to locate the valence and conduction levels. A convenient means is to excite QW photoluminescence by circularly polarized light. In this situation the light helicity is transferred to the solid through spin orientation of the promoted electrons.² This leads to circular polarization of the luminescence light, which depends on the initial valence state and on spin relaxation. For circularly polarized σ^+ excitation, the circular polarization \mathcal{P} of luminescence is defined by

$$\mathcal{P} = (I_+ - I_-)/(I_+ + I_-),$$

where I_+ (I_-) is the σ^+ (σ^-) circularly polarized luminescence intensity.

In many experiments³⁻⁶ a high polarization \mathcal{P} (30% $< \mathcal{P} < 60\%$) is observed for near-band-gap excitation, followed by a negative dip for larger excitation energy. The different signs of polarization are attributed to the different optical transitions: $a+100\%$ polarization is predicted for the $1h$ transition between the $n=1$ heavy-hole and conduction levels and $a-100\%$ polarization for the $1l$ ($n=1$ light hole to conduction) transition. This fact is used to identify the heavy- or light-hole transition.⁴ However, in the simplest parabolic model of the QW valence bands, because of the relative densities of states of the heavy- and light-hole bands, the net polarization remains positive for all excitation energies: $\mathcal{P}=100\%$ for $1h$ transition and $\mathcal{P}\approx 60\%$ at the excitation energy E_{1lc} corresponding to the onset of the $1l$ transition,⁵ in contrast with the experimental results. In the present paper we show that taking into account the valence-band nonparabolicity allows prediction of a behavior of \mathcal{P} in qualitative agreement with the experiments.

For that purpose, we need to calculate the optical matrix elements between valence and conduction states under circularly polarized light excitation. Since the wave functions necessary to calculate these optical transitions are

not explicitly given in the literature, Sec. I is devoted to the calculation of energy dispersion and wave functions in a simple variational approach. In Sec. II we calculate the polarization of the excitation spectrum, and comment on the results, in particular on spin relaxation and damping effect.

I. BAND STRUCTURE

The starting point of our calculation consists in finding wave functions and band structure near the bottom of the conduction and the top of the valence bands. We use here the effective-mass method, the so-called envelope-function approximation.^{7,8} In this approximation the conduction ($\alpha=c$) or valence ($\alpha=v$) wave function of the carrier in a QW has the form

$$\Psi^\alpha(\mathbf{r}) = \sum_{i=1}^{l_\alpha} F_i^\alpha(\mathbf{r}) u_{i,\mathbf{k}=0}^\alpha(\mathbf{r}), \quad (1)$$

where $u_{i,\mathbf{k}=0}^\alpha(\mathbf{r})$ is the periodic part of the Bloch wave function taken at the bottom ($\alpha=c$) or top ($\alpha=v$) of the band and $F_i^\alpha(\mathbf{r})$ is a multicomponent envelope function which satisfies a set of equations⁸

$$\sum_{i=1}^{l_\alpha} [H_{ij}^\alpha(-i\nabla) + V^\alpha(\mathbf{r})\delta_{ij}] F_i^\alpha(\mathbf{r}) = E F_j^\alpha(\mathbf{r}), \quad (2)$$

where $H(\mathbf{k})$ is a standard effective mass Hamiltonian, $V^\alpha(\mathbf{r})$ the well potential, and α stands for conduction or valence bands ($l_c=2$, $l_v=4$).⁹ Atomic units are used.

The usual QW growth direction is parallel to one of the cubic axes, and we take it for z direction. Then we have

$$H^\alpha(-i\nabla) = H^\alpha(k_x, k_y, -i(\partial/\partial z)),$$

$$V^\alpha(\mathbf{r}) = V^\alpha(z),$$

and

$$F_i^\alpha(\mathbf{r}) = e^{ik_x x} e^{ik_y y} \Phi_i^\alpha(z).$$

A. Valence band

For the valence band the standard Luttinger Hamiltonian¹⁰ in the basis $|\frac{3}{2}, \frac{3}{2}\rangle, |\frac{3}{2}, -\frac{1}{2}\rangle, |\frac{3}{2}, \frac{1}{2}\rangle, |\frac{3}{2}, -\frac{3}{2}\rangle$ reads as follows:

$$H(k_x, k_y, k_z) = \begin{pmatrix} P+Q & R & -S & 0 \\ R^* & P-Q & 0 & S \\ -S^* & 0 & P-Q & R \\ 0 & S^* & R^* & P+Q \end{pmatrix}, \quad (3)$$

where

$$\begin{aligned} P &= \frac{1}{2}\gamma_1(k_x^2 + k_y^2 + k_z^2), \\ Q &= \frac{1}{2}\gamma_2(k_x^2 + k_y^2 - 2k_z^2), \\ S &= \sqrt{3}\gamma_3 k_z(k_x - ik_y), \\ R &= -(\sqrt{3}/2)\bar{\gamma}(k_x^2 - k_y^2) \\ &\quad + (\sqrt{3}/2)[\frac{1}{2}(\gamma_3 - \gamma_2)](k_x + ik_y)^2, \end{aligned}$$

and $\gamma_1, \gamma_2, \gamma_3$, and $\bar{\gamma} = \frac{1}{2}(\gamma_2 + \gamma_3)$ are the Luttinger band parameters.

Following the idea of Broido and Sham¹¹ we transform the Hamiltonian (3) by a unitary transformation U into

$$\bar{H}(k_x, k_y, k_z) = UHU^\dagger = \begin{pmatrix} P+Q & \tilde{R} & 0 & 0 \\ \tilde{R}^* & P-Q & 0 & 0 \\ 0 & 0 & P-Q & \tilde{R} \\ 0 & 0 & \tilde{R}^* & P+Q \end{pmatrix}, \quad (4)$$

$$\left[\begin{array}{cc} \frac{1}{2}(\gamma_1 \pm \gamma_2)k_{\parallel}^2 - \frac{1}{2}(\gamma_1 \mp 2\gamma_2)\frac{\partial^2}{\partial z^2} + V(z) & (\sqrt{3}/2)\bar{\gamma}k_{\parallel}^2 - \sqrt{3}\gamma_3 k_{\parallel} \frac{\partial}{\partial z} \\ (\sqrt{3}/2)\bar{\gamma}k_{\parallel}^2 - \sqrt{3}\gamma_3 k_{\parallel} \frac{\partial}{\partial z} & \frac{1}{2}(\gamma_1 \mp \gamma_2)k_{\parallel}^2 - \frac{1}{2}(\gamma_1 \pm 2\gamma_2)\frac{\partial^2}{\partial z^2} + V(z) \end{array} \right], \quad (6)$$

where the upper (lower) sign refers to the $|1\rangle, |2\rangle, (|3\rangle, |4\rangle)$ block in (4).

Our calculation is variational in its principle. We successively consider the cases $k_{\parallel} = 0$ and finite k_{\parallel} . We first notice that for $k_{\parallel} = 0$ each block of Hamiltonian (6) becomes diagonal with elements

$$\begin{aligned} H_h &= -\frac{1}{2}(\gamma_1 - 2\gamma_2)\frac{\partial^2}{\partial z^2} + V(z), \\ H_l &= -\frac{1}{2}(\gamma_1 + 2\gamma_2)\frac{\partial^2}{\partial z^2} + V(z), \end{aligned} \quad (7)$$

yielding a set of doubly degenerate heavy- (subscript h) and light-hole (subscript l) subband energies. For a finite square well of width L equations (7) have well-known solutions ϕ_i^h and ϕ_i^l , where h and l correspond to H_h and H_l , respectively (see Appendix B).

Then for finite k_{\parallel} we return to Hamiltonian (6) and construct envelope functions as linear combinations of ϕ_i

where $\tilde{R} = |R| - i|S|$.

The original basis function set and transformation U are given in Appendix A. The new basis is now

$$\begin{aligned} |1\rangle &= a|\frac{3}{2}, \frac{3}{2}\rangle - a^*|\frac{3}{2}, -\frac{3}{2}\rangle, \\ |2\rangle &= b|\frac{3}{2}, -\frac{1}{2}\rangle - b^*|\frac{3}{2}, \frac{1}{2}\rangle, \\ |3\rangle &= b|\frac{3}{2}, -\frac{1}{2}\rangle + b^*|\frac{3}{2}, \frac{1}{2}\rangle, \\ |4\rangle &= a|\frac{3}{2}, \frac{3}{2}\rangle + a^*|\frac{3}{2}, -\frac{3}{2}\rangle, \end{aligned} \quad (5)$$

where a and b are given in Appendix A. It should be noticed that functions (5) still have pure heavy- or light-hole character. For further analysis we apply here the so-called axial approximation. This approximation has been shown⁸ to give a good description of the valence subbands energy dispersion and consists in assuming $\gamma_2 = \gamma_3$, but only in the R term. Thus we neglect the warping of the bulk valence band only in the (k_x, k_y) plane. The Hamiltonian expression (3) remains exact for $k_x, k_y = 0$ and therefore produces the exact subband positions at this point. In contrast the spherical approximation, in which γ_2 and γ_3 are replaced by a suitable average $\gamma' = (3\gamma_3 + 2\gamma_2)/5$ (Ref. 12) everywhere in (3), neglects the warping of the bulk valence band in all directions and produces substantial errors in the $k_x, k_y = 0$ subband energies.¹³ We will return to this point later.

Since Hamiltonian (4) acquires cylindrical z symmetry we may take $k_x = k_{\parallel}$ and $k_y = 0$. Therefore the effective Hamiltonian in (2),

$$H_{\text{eff}} = H(k_x = k_{\parallel}, k_y = 0, k_z = -i(\partial/\partial z)) + V(z),$$

reduces into two blocks which read

$$\Phi^h(z) = \sum_{i=1}^{l_h} a_i \phi_i^h(z), \quad \Phi^l(z) = \sum_{i=1}^{l_l} b_i \phi_i^l(z), \quad (8)$$

a_i and b_i being numerical coefficients and l_h (l_l) the total number of bound heavy (light) states in the well. The above wave functions, in which the band indices are omitted for clarity, satisfy the same continuity relations as the basis functions ϕ_i : ϕ_i and $(1/m_{l,h})(\partial\phi_i/\partial z)$ continuous at the well interface, with $m_{l,h} = (\gamma_1 \pm 2\gamma_2)^{-1}$. Since we limit the above expansion to bound states our basis is not complete and, moreover, we are limited by the number of available states in the particular QW. Therefore for a QW with a small number of bound states (i.e., rather narrow and shallow) one may expect increasing errors in energy dispersion for large k_{\parallel} (especially for higher subbands). However, as will be shown in Sec. II, the most spectacular effects in polarization spectra are due to the electrons created with $k_{\parallel} \cong 0$. Thus the incompleteness of our basis practically does not influence the calculated polarization

spectra even for QW's with very few bound states. Finally the total wave functions read

$$\begin{aligned}\Psi_{1,2} &= e^{ik_{\parallel}x} \Phi_{1,2}^h |1\rangle + e^{ik_{\parallel}x} \Phi_{1,2}^l |2\rangle, \\ \Psi_{3,4} &= e^{ik_{\parallel}x} \Phi_{3,4}^l |3\rangle + e^{ik_{\parallel}x} \Phi_{3,4}^h |4\rangle.\end{aligned}\quad (9)$$

The general boundary conditions for the many-band envelope functions (9) (derived from the probability current conservation conditions or by integrating the Hamiltonian across the interface) are exactly fulfilled in our case only for $k_{\parallel}=0$. For finite k_{\parallel} , however, our variational procedure leads to the coefficients a_i, b_i , so that $\Psi_{1,2}$ and $\Psi_{3,4}$ approximate the real wave functions and in the same way satisfy the true boundary conditions as well as possible in this finite basis. We have performed a numerical diagonalization of the Hamiltonian matrix (6) (given explicitly in Appendix C) and obtained the valence-band structure $E(k_{\parallel})$ and the wave-function coefficients a_i, b_i .

In Fig. 1 we show the results for a 140-Å-thick GaAs well between $\text{Ga}_{0.79}\text{Al}_{0.21}\text{As}$ barriers. Band parameter values for GaAs and AlAs are listed in Table I (after Ref. 14), those for $\text{Ga}_{0.79}\text{Al}_{0.21}\text{As}$ being obtained by linear interpolation. The most important parameter is the valence well depth V_0^v . This parameter is determined by the difference between energy gaps of the well and barrier materials ($\Delta E_g = \Delta E_c + \Delta E_v$) and the offset parameter $Q_c = \Delta E_c / \Delta E_g$. Since different authors report different

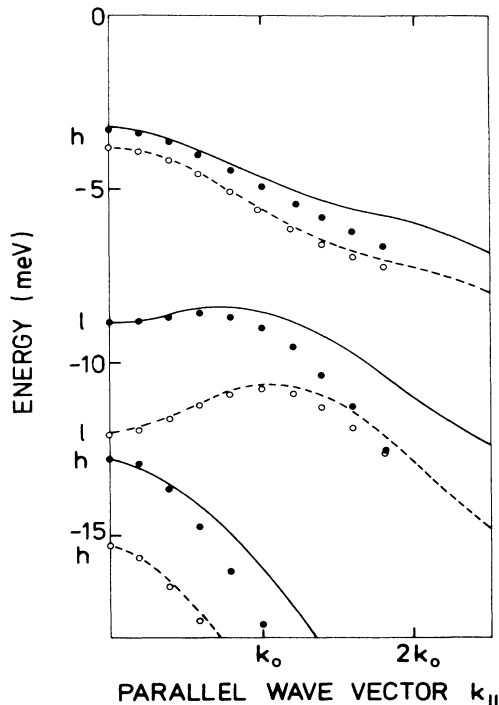


FIG. 1. Valence-band energy dispersion for a GaAs/ $\text{Ga}_{0.79}\text{Al}_{0.21}\text{As}$ 140-Å QW, calculated in the axial approximation for two-band offset parameters: $Q_c=0.57$ (open circle) and $Q_c=0.85$ (solid circle). The results of Altarelli *et al.* (Ref. 8) are plotted for comparison: $Q_c=0.57$ (dashed line) and $Q_c=0.85$ (solid line). h and l denote heavy- and light-hole character at $k_{\parallel}=0$, k_0 stands for $k_{\parallel}=\pi/340$ Å.

TABLE I. Band parameters of GaAs and AlAs in atomic units (from Ref. 14). $E_g(\text{Ga}_{1-x}\text{Al}_x\text{As}) = E_g(\text{GaAs}) + 1.04x + 0.47x^2$ for $x < 0.4$.

	GaAs	AlAs
m_e	0.067	0.124
γ_1	6.85	3.45
γ_2	2.10	0.68
γ_3	2.90	1.29
E_g (eV)	1.520	3.13

Q_c values¹⁵ we present here results for $Q_c=0.57$ (Ref. 16) and $Q_c=0.85$ (Ref. 17).

It can be noticed that our results are in good agreement with extended computations by Altarelli *et al.*⁸ (Fig. 1). We are not going to discuss in details the QW valence-band structure which was already investigated by many authors,^{8,18} we rather point out the most important features of this structure.

In $k_{\parallel}=0$ heavy and light holes exactly decouple as discussed earlier, and it is therefore possible to label subbands as “heavy” or “light” according to their $k_{\parallel}=0$ character. For finite k_{\parallel} the admixture of light- (heavy-) hole function into heavy- (light-) hole state becomes significant as shown in Fig. 2. This results in characteristic nonparabolicities which may be observed in Fig. 1 (negative mass of the first light-hole subband for $k \sim 0$ and reversal of its sign for $k \sim \pi/2L$, where L is the well width). Since for small k the light-hole mass has the same sign as the electron mass, this leads to high joint density of states (JDOS). For large k_{\parallel} ($\sim \pi/L$) our results deviate from

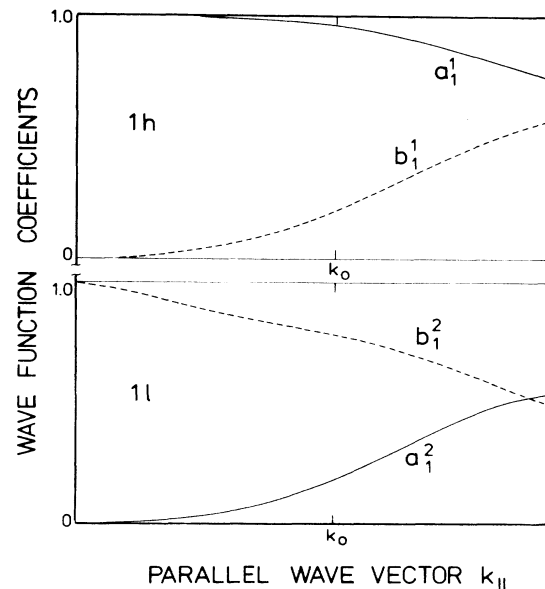


FIG. 2. Dominant components of the first ($1h$, upper part) and the second ($1l$, lower part) valence subband wave functions on the ϕ_i^h and ϕ_i^l basis. The coefficients a_i (b_i) expresses the admixture of ϕ_i^h (ϕ_i^l) basis functions into the total subband wave functions for increasing k_{\parallel} . For $k_{\parallel}=0$ the $1h$ ($1l$) wave function has pure heavy- (light-) hole character.

those of Altarelli *et al.*⁸ This is mainly due to the limited number of basis functions used in the present example: There exist six heavy-hole (h) levels and three light-hole (l) levels for $Q_c=0.57$ (the QW depth is $V_0^v=103$ meV) and only three h and two l levels for $Q_c=0.85$ ($V_0^v=36$ meV).

The same type of variational calculation in the axial approximation has been performed for another QW system, namely $\text{Ga}_{0.47}\text{In}_{0.53}\text{As}$ well with InP barriers. The energy dispersions calculated using the parameters from Table II (Refs. 19–22) and a band offset $Q_c=0.57$ are presented in Fig. 3. As compared to the $\text{GaAs}/\text{Ga}_{1-x}\text{Al}_x\text{As}$ case shown in Fig. 1, one may observe similar nonparabolicities of the valence subbands, but the most distinguishing features is the different order of these bands. For $\text{Ga}_y\text{In}_{1-y}\text{As}/\text{InP}$ the $1h$ subband is followed by the $2h$ band, the $1l$ subband being only the third one.

Finally, we would like to comment on the spherical approximation. In the case of $\text{GaAs}/\text{Ga}_{0.79}\text{Al}_{0.21}\text{As}$ discussed earlier the replacement of γ_2 and γ_3 by $\gamma'=(2\gamma_2+3\gamma_3)/5$ leads to a wrong subband sequence: $1h, 2h, 1l, 3h, \dots$, instead of $1l, 2h, 3h, \dots$, obtained in the axial approximation. Thus the spherical approximation is not only quantitatively but even qualitatively incorrect.

It is also worth noticing that the infinite well approximation also leads to an incorrect ordering of the valence subbands. Therefore those approximations cannot be used in our problem.

B. Conduction band

We consider the conduction band as decoupled from the valence bands. In the envelope-function framework the conduction-band effective Hamiltonian for a QW is diagonal in the $|J, J_z\rangle$ basis and is given by

$$H_{\text{eff}}^c = (1/2m_e)[k_{\parallel}^2 - (\partial^2/\partial z^2)] + V^c(z)$$

where m_e is the electron effective mass. The conduction band consists of a set of doubly degenerate states:

$$\Psi^c = \phi^c(z) e^{ik_{\parallel}x} \left| \frac{1}{2}, \pm \frac{1}{2} \right\rangle, \quad (10)$$

where $\left| \frac{1}{2}, +\frac{1}{2} \right\rangle = |s\uparrow\rangle$, $\left| \frac{1}{2}, -\frac{1}{2} \right\rangle = |s\downarrow\rangle$, and ϕ^c are functions analogous to the valence band functions (see Appendix B; $m_{h,l}$ masses are substituted by m_e and V_0^v by $V_0^c = \Delta E_g Q_c$). The conduction-band dispersion is given

TABLE II. Band parameters of $\text{Ga}_{0.47}\text{In}_{0.53}\text{As}$ (Ref. 19) and InP (Refs. 20 and 21) in atomic units deduced from cyclotron resonance experiments. Parameters γ_1 , γ_2 , and γ_3 for $\text{Ga}_y\text{In}_{1-y}\text{As}$ are obtained by linear interpolation of GaAs (Ref. 11) and InAs (Ref. 22) values.

	$\text{Ga}_{0.47}\text{In}_{0.53}\text{As}$	InP
m_e	0.041	0.079
γ_1	13.95	5.04
γ_2	5.69	1.56
γ_3	6.07	1.73
E_g (eV)	0.812	1.425

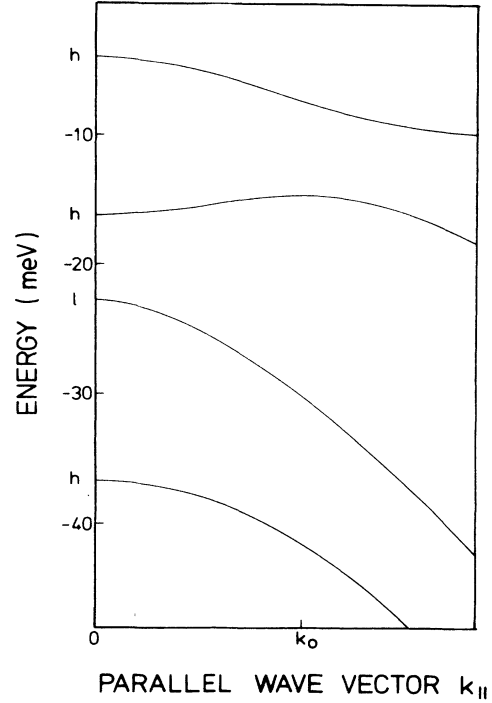


FIG. 3. Valence-band energy dispersion for a $\text{Ga}_{0.47}\text{In}_{0.53}\text{As}/\text{InP}$ 140-Å QW calculated in the axial approximation with a band offset $Q_c=0.57$. k_0 stands for $k_{\parallel} = \pi/340$ Å, h and l indicate heavy- or light-hole character at $k_{\parallel}=0$.

by

$$E_i^c(k_{\parallel}) = \epsilon_i^c + \frac{1}{2m_e} k_{\parallel}^2, \quad (11)$$

ϵ_i^c being the bound-state energies of the conduction band well for $k_{\parallel}=0$.

II. POLARIZATION OF PHOTOLUMINESCENCE

A. Calculation

In this section we will calculate the circular polarization of the photoluminescence excitation spectrum. The considered process is the following (Fig. 4): excitation of electrons from valence subbands to the lowest ($1c$) conduction subband,²³ relaxation of photocreated electrons and holes to the bottom of conduction band and top of the valence band, respectively, and recombination of relaxed electrons to the highest valence subband ($1h$).

We make the following simplifying assumptions: (i) We neglect excitonic effects (i.e., electron-hole Coulomb interaction). All transitions are considered to be band-to-band. (ii) Holes are supposed to completely relax their spin during energy relaxation. This is indeed the case in bulk material because of scattering between light- and heavy-hole bands.² However, when heavy-hole and light-hole bands are decoupled by uniaxial stress²⁴ or crystal field,²⁵ it is known that the hole spin relaxation is much reduced.

Let us show *ad absurdum* that in QW's the hole spin relaxation remains important. Suppose that, because of the valence bands decoupling, the hole spin relaxation is

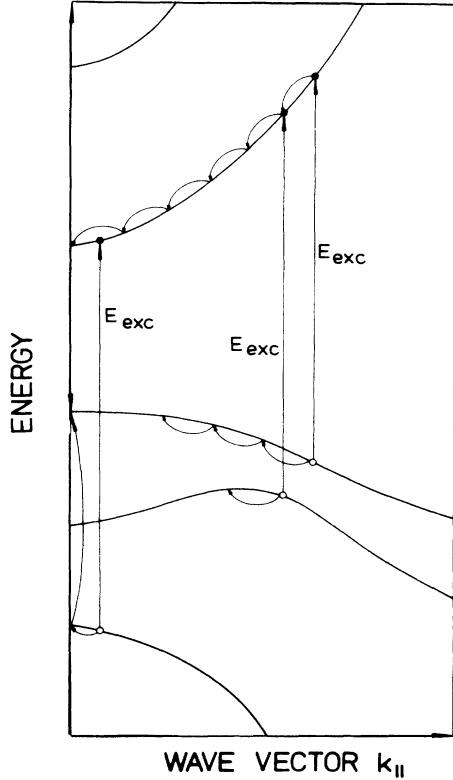


FIG. 4. Schematic QW band structure and transition schemes discussed in Sec. II.

canceled. Then the luminescence polarization is +100%: If the only available holes originate from the absorption process, the electrons can only recombine to the same valence states they were promoted from. This is even true in the presence of electron spin relaxation because in the recombination process the hole selects the spin of the recombining electron. Since the experimental determinations of the luminescence polarization are at most 60% (Refs. 3–6) the hole spin relaxation cannot be canceled. Thus our assumption describes in a simplified way the fact that hole spin relaxation is present, probably due to the fact that the valence Γ_8 states have cubic and not vectorial symmetry. It should be noticed that our hypothesis of *total* hole spin relaxation will lead, versus the exciting photon energy, to the largest deviation from the constant +100% value for polarization.

We first calculate the luminescence polarization assuming no spin depolarization in the conduction band. This spin depolarization will be discussed in Sec. II C. The circular polarization of photoluminescence is calculated in the density matrix formalism.²⁶ For σ^+ (σ^-) light excitation the density operator describes the state of photocreated electrons and reads

$$\rho^\pm = \sum_i p^\pm |\Psi_i^\nu\rangle \langle \Psi_i^\nu | p^\mp, \quad (12)$$

where p^\pm is the dipole transition operator for σ^+ and σ^- light and $|\Psi_i^\nu\rangle$ are the initial valence states described by wave functions (9) from which electrons were promoted; in our case each valence subband is doubly degenerate. Note that ρ is not normalized to unity but rather to the density of excited carriers with a given $k_{||}$. Since we consider thermalized recombination from the bottom of the conduction subband, we must take into account electrons created with all possible $k_{||}$. That means averaging ρ over all possible directions of $k_{||}$. Finally for photoexcitation of an electron from the j th valence subband into the first conduction subband we obtain the average ρ density matrices [calculated on the first conduction subband states (10)]:

$$\begin{aligned} \tilde{\rho}_j^+ &= \frac{2}{3} P^2 g_j \begin{pmatrix} \sum_{i=1}^{l_l} |b_i^j|^2 |S_{1i}^{cl}|^2 & 0 \\ 0 & 3 \sum_{i=1}^{l_h} |a_i^j|^2 |S_{1i}^{ch}|^2 \end{pmatrix}, \\ \tilde{\rho}_j^- &= \frac{2}{3} P^2 g_j \begin{pmatrix} 3 \sum_{i=1}^{l_h} |a_i^j|^2 |S_{1i}^{ch}|^2 & 0 \\ 0 & \sum_{i=1}^{l_l} |b_i^j|^2 |S_{1i}^{cl}|^2 \end{pmatrix}, \end{aligned} \quad (13)$$

where $P = \langle X | p | S \rangle$ is the valence-to-conduction interband matrix element, a_i, b_i are the coefficients of wave functions (9), $S_{1i}^{cl} = \langle \phi_1^c | \phi_i^l \rangle$, $S_{1i}^{ch} = \langle \phi_1^c | \phi_i^h \rangle$ are overlap integrals between basis functions, and $g_j = (1/\pi) k_{||} (\partial k_{||} / \partial E_{exc})$ is the joint density of states for the considered transition expressed in atomic units (E_{exc} being the excitation energy). The total density matrix for transitions from several valence subbands is then $\tilde{\rho} = \sum_j \tilde{\rho}_j$. The recombination (Fig. 4) into first valence subband ($1h$) ($k_{||}=0$, $a_i^j = \delta_{1i}$, $b_i^j = 0$) is described by

$$\begin{aligned} \tilde{\rho}_{k_{||}=0}^+ &= \frac{1}{2} P^2 g_1 \begin{pmatrix} 0 & 0 \\ 0 & 4 |S_{11}^{ch}|^2 \end{pmatrix}, \\ \tilde{\rho}_{k_{||}=0}^- &= \frac{1}{2} P^2 g_1 \begin{pmatrix} 4 |S_{11}^{ch}|^2 & 0 \\ 0 & 0 \end{pmatrix}. \end{aligned} \quad (14)$$

The σ^+, σ^- luminescence intensities (under σ^+ excitation) are obtained by calculating the following traces:²⁶

$$\begin{aligned} I_+ &= \text{Tr}(\tilde{\rho}^+ \tilde{\rho}_{k_{||}=0}^+), \\ I_- &= \text{Tr}(\tilde{\rho}^+ \tilde{\rho}_{k_{||}=0}^-). \end{aligned} \quad (15)$$

Then the luminescence polarization is given by

$$\mathcal{P}_0 = \frac{I_+ - I_-}{I_+ + I_-} = \frac{3 \sum_j g_j \left[\sum_{i=1}^{l_h} |a_i^j|^2 |S_{1i}^{ch}|^2 \right] - \sum_j g_j \left[\sum_{i=1}^{l_l} |b_i^j|^2 |S_{1i}^{cl}|^2 \right]}{3 \sum_j g_j \left[\sum_{i=1}^{l_h} |a_i^j|^2 |S_{1i}^{ch}|^2 \right] + \sum_j g_j \left[\sum_{i=1}^{l_l} |b_i^j|^2 |S_{1i}^{cl}|^2 \right]}. \quad (16)$$

B. Results

We now present the polarization excitation spectra calculated according to formula (16) on the basis of numerical diagonalization of Hamiltonian (6) for different cases. The excitation polarization spectrum resulting from the band structure presented in Fig. 1 (GaAs/Ga_{0.79}Al_{0.21}As, $L=140$ Å, $Q_c=0.57$, axial approximation) is shown in the upper part of Fig. 5. In the energy range $E_{\text{exc}} < E_{1lc}$ ($n=1$ light-hole-to-conduction transition) only electrons from the first valence subband are created in the conduction band. Since the first valence subband has mainly heavy-hole character (cf. Fig. 2) the resulting photoluminescence polarization is positive and close to +100%. The small decrease to 95% is due to a small light-hole admixture in the $1h$ wave function. For an excitation energy exceeding E_{1lc} the electrons from the second valence subband start to contribute to the luminescence. These electrons originate from the light-hole-type subband (Fig. 2) and carry a -100% polarization. The joint density of states (JDOS) for this transition is very high (Fig. 5, lower part), resulting in a net negative polarization as strong as -78%. Note that for such an excitation energy electrons promoted from the $1h$ subband have

$k_{\parallel} \cong 5 \times 10^{-3} \text{ \AA}^{-1} \cong k_0$, a relatively small value for which our calculation of band structure does not significantly deviate from the exact one (see Fig. 1).

As the excitation energy increases the JDOS for the $1l \rightarrow 1c$ transition falls down: Although the wave function still retains its light-hole character the net polarization then becomes positive. It should be stressed that coincidence of both large JDOS and light-hole character of photoexcited electrons is necessary for negative polarization.

For still higher excitation energies ($E_{\text{exc}} > E_{2h \rightarrow 1c}$) electrons from the third valence subband appear in the conduction band. The wave function of these $2h$ electrons is mainly built of ϕ_2 basis function. Thus $S_{12}^{ch} = \langle \phi_1^c | \phi_2^h \rangle = 0$ because of different parities of ϕ_1^c and ϕ_2^h , so that these electrons negligibly contribute to the absorption process and consequently to the polarization as can be seen in Fig. 5.

The influence of the well depth on polarization spectra essentially enters through the modification of the JDOS for the light-hole transition: The deeper the well, the higher the JDOS, and the more negative the polarization at the onset of the light-hole transition. In Fig. 6 (upper part) the excitation spectrum is shown for the same QW except that $Q_c=0.85$. The valence-band well depth is now only 36 meV, which results in much lower JDOS for the $1l \rightarrow 1c$ transition (Fig. 6 lower part). Hence, in spite of the light-hole character of electrons created at the onset of this transition, the polarization remains positive for all energies. The $2h \rightarrow 1c$ transition negligibly contribute to the polarization for the same reasons as discussed above. On the other hand for an unrealistic value $Q_c=0.3$ the

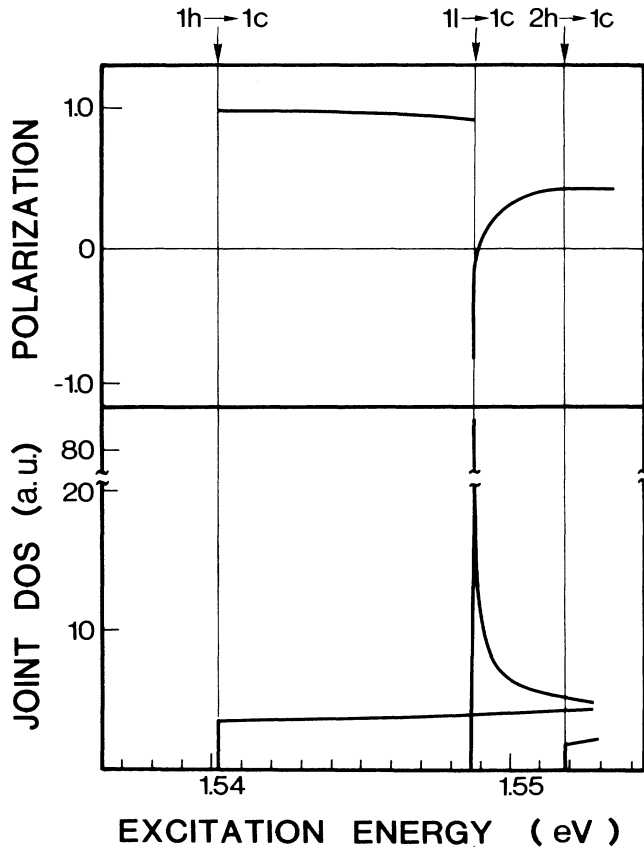


FIG. 5. Excitation spectrum of the luminescence circular polarization (upper part) and joint density of states (lower part) for a 140-Å GaAs/Ga_{0.79}Al_{0.21}As QW in the axial approximation with $Q_c=0.57$. The arrows denote the onsets of $1h \rightarrow 1c$, $1l \rightarrow 1c$, and $2h \rightarrow 1c$ transitions.

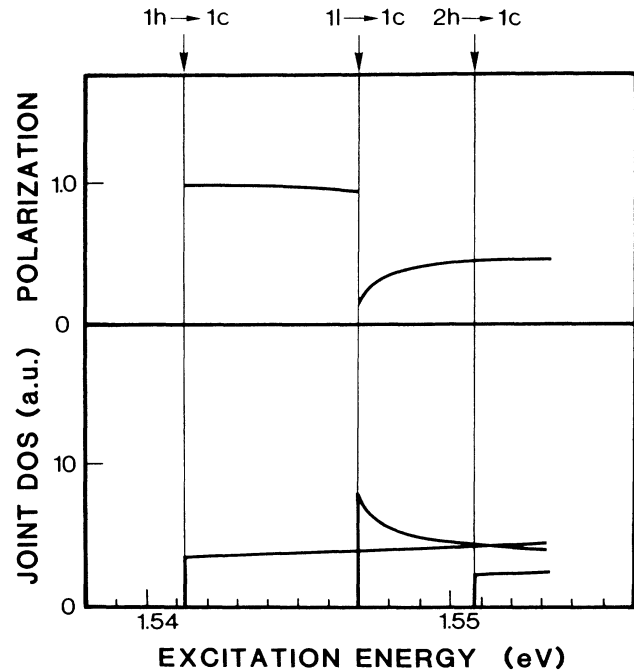


FIG. 6. Excitation spectrum of the luminescence circular polarization (upper part) and joint density of states (lower part) for the same system as in Fig. 5 except that now $Q_c=0.85$.

valence-band well is deeper and this case is essentially similar to the situation for $Q_c=0.57$: high JDOS for $1l \rightarrow 1c$ transitions and negative polarization (slightly more negative than for $Q_c=0.57$).

We have also calculated the polarization spectrum for the $\text{Ga}_{0.47}\text{In}_{0.53}\text{As}/\text{InP}$ system using the band structure shown in Fig. 3. The results are plotted in Fig. 7. As was previously noticed the first two valence-band levels have heavy-hole character; only the third band is a light-hole band. The high peak in JDOS is still present but now corresponds to transitions from $2h$ subband. The wave function of this subband mainly consists of ϕ_2 function ($a_2=0.965$ at $k_{\parallel}=0$) having heavy-hole character. However, as was mentioned, optical transitions $\phi_2^{h,l} \rightarrow \phi_1^c$ are forbidden and do not contribute to the polarization, which is then dominated by the light-hole admixture ($b_1=0.15$ at $k_{\parallel}=0$) of the $2h$ wave function. Since the JDOS is much higher than for $1h \rightarrow 1c$ transition, we consequently observe a steplike polarization decrease around $E_{\text{exc}}=E_{2h \rightarrow 1c}$. The true light-hole-type electrons are promoted from the third valence subband ($1l$), but the

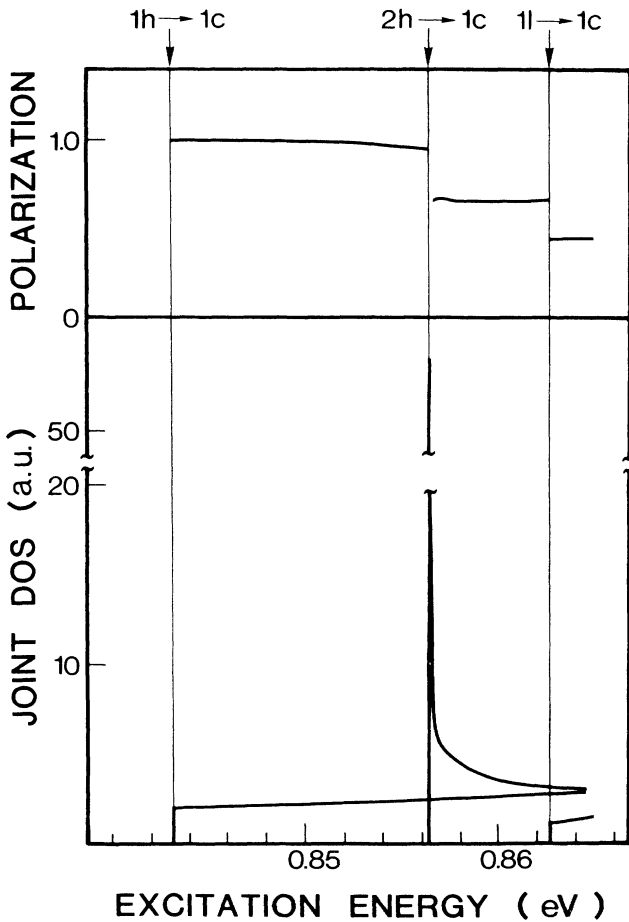


FIG. 7. Excitation spectrum of the luminescence circular polarization (upper part) and joint density of states (lower part) for a 140-Å $\text{Ga}_{0.47}\text{In}_{0.53}\text{As}/\text{InP}$ QW in the axial approximation with $Q_c=0.57$. The arrows denote the onsets of $1h \rightarrow 1c$, $2h \rightarrow 1c$, and $1l \rightarrow 1c$ transitions.

JDOS for this transition is too small to result in negative polarization and only a weak decrease of \mathcal{P} is observed. The spherical approximation discussed in Sec. I for $\text{GaAs}/\text{Ga}_{1-x}\text{Al}_x\text{As}$ leads to polarization spectra similar to that for $\text{Ga}_y\text{In}_{1-y}\text{As}/\text{InP}$ (i.e., no negative polarization) because of the same order of the first valence levels.

We summarize the above results as follows: Negative polarization of excitation spectra may be expected for the transitions from the light-hole-type valence subbands, but only if combined with large joint density of states. That may be achieved for sufficiently deep QW's with appropriate valence-subband sequence ($1h$ immediately followed by $1l$ subband).

C. Discussion

So far we have neglected spin relaxation in the conduction band. Obviously this effect should be included in the calculations [all experiments report polarization smaller than 100% (Refs. 3–6)]. In the considered optical process, electron spin relaxation can occur both during the energy relaxation and in the thermalized state at the bottom of conduction band before the recombination.^{27,28} The exact relaxation mechanisms in two-dimensional (2D) systems are not known up to now. However, we may predict the influence of electron spin relaxation on the shape of polarization excitation spectra. The depolarization in the thermalized state will decrease \mathcal{P} without changing the overall spectrum shape [$\mathcal{P} = \mathcal{P}_0 \tau_S / (\tau_S + \tau)$, where τ_S is the electron spin relaxation time and τ is the electron lifetime²]. The depolarization during thermalization depends on the ratio of the energy relaxation time to the spin relaxation time^{27,28} and increases with kinetic energy of photocreated electrons. This means that if electrons are promoted from a single subband ($1h \rightarrow 1c$ transition) the polarization decreases with increasing excitation energy. Thus at the onset of $1l$ electrons excitation to the bottom of the conduction band, the weight of the $1h \rightarrow 1c$ transition in the polarization is weakened. This will change the shape of the polarization spectrum, enhancing its negative part (for $\text{GaAs}/\text{GaAlAs}$ QW).

One may expect that in real experimental situations the above sharp excitation spectra will be broadened. That may be due, for instance, to growth imperfections of QW wafers: small macroscopic variations of barrier composition or well depth will cause small changes of QW energy levels²⁹ that will result in broadening of polarization spectra.

We have simulated such a broadening in the absence of conduction spin relaxation by convolution of the spectrum in Fig. 5 with a Gaussian function

$$G(x, \gamma) = (\gamma \sqrt{\pi L n 2})^{-1} \exp[-(x/\gamma \sqrt{L n 2})^2],$$

where γ is the damping parameter. The results for $\gamma=0.05$ and 0.20 meV are shown in Fig. 8. It should be noticed that the excitation spectrum is very sensitive to such a broadening which may even cancel negative polarization for $\gamma > 1$ meV.

Indeed in the reported experiments for GaAs QW's (Refs. 3–6) the overall shape (high positive polarization followed by a negative minimum and then positive polari-

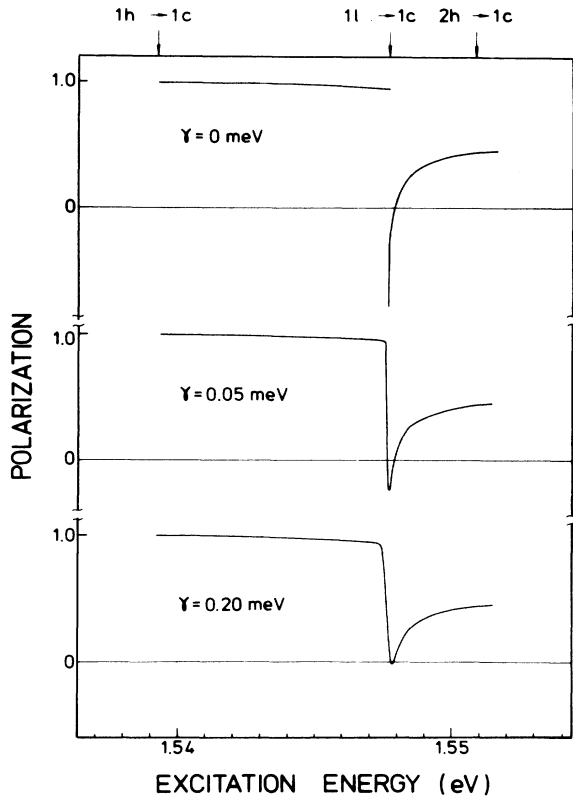


FIG. 8. Effects of broadening on the excitation spectrum shown in Fig. 5 for the damping parameter values $\gamma=0$ meV, 0.05 meV, and 0.20 meV, respectively.

zation) is in agreement with our results. However, the width of the negative dip is of the order of a few meV. This is much larger than in our calculations and yet negative polarization is still observed. This evidences the role of conduction electron spin relaxation.

We therefore think that at the present stage any comparison of our results with experiments can only be qualitative. The calculated spectra strongly depend on such material parameters as barrier compositions, offset value Q_c , well width, broadening and spin relaxation, i.e., too many parameters to make reasonable fits.

CONCLUSION

We have performed the first calculation of the circular polarization of the luminescence excitation spectrum of a QW system, which reflects the features of experimental structures: high positive polarization for $1h \rightarrow 1c$ transition, negative polarization for $1l \rightarrow 1c$ transition. This negative polarization directly results from the nonparabolicity of the QW valence band and requires proper ordering of valence subbands: $1h$ level followed by $1l$ level. Such a situation is encountered in GaAs/GaAlAs with sufficiently deep valence wells. For the other systems, with different valence subband sequence ($1h, 2h, 1l, 3h \dots$) as in $\text{Ga}_{0.47}\text{In}_{0.53}\text{As}/\text{InP}$ the polarization remains positive, only presenting decreasing steps with increasing excitation energy.

At the present stage we believe that a direct comparison with experimental data is meaningless because of the too large number of QW parameters, critical for the exact shape of polarization spectra, which are not accurately known. Therefore improvements are required in two ways: on the one hand, better controlled samples are necessary, on the other hand a theory of 2D excitons in systems with complicated degenerate valence band like GaAs QW should be elaborated and then could be applied to the photoluminescence polarization calculations.

ACKNOWLEDGMENTS

We wish to thank Dr. J. A. Gaj and Dr. J. Blinowski for helpful discussions, and Dr. G. Lampel and Dr. D. Paget for a critical reading of the manuscript. Laboratoire de Physique de la Matière Condensée is Groupe de Recherche No. 38 du Centre National de la Recherche Scientifique, France.

APPENDIX A

The basis set for the matrix (3) is the $|J, J_z\rangle$ basis for $J = \frac{3}{2}$:

$$|\frac{3}{2}, \frac{3}{2}\rangle = -(1/\sqrt{2})|(X+iY)\uparrow\rangle,$$

$$|\frac{3}{2}, -\frac{1}{2}\rangle = (1/\sqrt{6})|(X-iY)\uparrow\rangle + (2/3)^{1/2}|Z\downarrow\rangle,$$

$$|\frac{3}{2}, -\frac{1}{2}\rangle = -(1/\sqrt{6})|(X-iY)\downarrow\rangle + (2/3)^{1/2}|Z\uparrow\rangle,$$

$$|\frac{3}{2}, -\frac{3}{2}\rangle = (1/\sqrt{2})|(X-iY)\downarrow\rangle.$$

The unitary transformation U is given by

$$U = \begin{pmatrix} \alpha^* & 0 & 0 & -\alpha \\ 0 & \beta & -\beta & 0 \\ 0 & \beta^* & \beta & 0 \\ \alpha^* & 0 & 0 & \alpha \end{pmatrix}$$

where

$$\alpha = (1/\sqrt{2})\exp[i(3\pi/4 - 2\phi/3)],$$

$$\beta = (1/\sqrt{2})\exp[i(-\pi/4 + \phi/2)],$$

and angle ϕ results from $\mathbf{k} = (k \sin\theta \sin\phi, k \sin\theta \cos\phi, k \cos\theta)$.

APPENDIX B

For a square-well potential

$$V(z) = \begin{cases} 0, & -L/2 < z < L/2, \\ V_0, & |z| > L/2, \end{cases}$$

the Hamiltonians (7), which differ only by the effective masses [$m = m_l = (\gamma_1 - 2\gamma_2)^{-1}$ for H_l and $m = m_h = (\gamma_1 + 2\gamma_2)^{-1}$ for H_h], have the following solutions:

for i even,

$$\phi_i(z) = \begin{cases} B_i \cos(k_i L/2) e^{\kappa_i L/2} e^{\kappa_i z}, & z < -L/2 \\ B_i \cos(k_i z), & -L/2 < z < L/2 \\ B_i \cos(k_i L/2) e^{-\kappa_i L/2} e^{-\kappa_i z}, & z > L/2; \end{cases}$$

for i odd,

$$\phi_i(z) = \begin{cases} -A_i \sin(k_i L/2) e^{\kappa_i L/2} e^{\kappa_i z}, & z < -L/2 \\ A_i \sin(k_i z), & -L/2 < z < L/2 \\ A_i \sin(k_i L/2) e^{\kappa_i L/2} e^{-\kappa_i z}, & z > L/2, \end{cases}$$

where

$$k_i = (2m_I \epsilon_i)^{1/2}, \quad \kappa_i = [2m_{II}(V_0 - \epsilon_i)]^{1/2}$$

ϵ_i being the eigenenergy. Subscripts I and II refer to $-L/2 < z < L/2$ (i.e., well material) and $|z| > L/2$ (i.e., barrier material), respectively.

A and B are normalization constants:

$$A_i = [L/2 - (1/2k_i)\sin(k_i L) + (1/\kappa_i)\sin^2(k_i L/2)]^{-1/2},$$

$$B_i = [L/2 + (1/2k_i)\sin(k_i L) + (1/\kappa_i)\cos^2(k_i L/2)]^{-1/2}.$$

Eigenenergies ϵ_i result from the continuity relations [ϕ_i and $(1/m)(\partial\phi_i/\partial z)$ continuous at the interface].

This treatment is successively applied to the heavy-hole levels ($m = m_h$) and to the light-hole levels ($m = m_l$), leading to the wave functions ϕ_i^h and ϕ_i^l and the corresponding eigenenergies for $k_{||} = 0$.

APPENDIX C

The Hamiltonian matrix (6) expressed in the ϕ_i basis is the following:

$$H = \begin{pmatrix} H^{11} & H^{12} \\ H^{21} & H^{22} \end{pmatrix},$$

where

$$H_{ij}^{11} = \frac{1}{2}(\gamma_1 + \gamma_2)k_{||}^2 \delta_{ij} + \epsilon_j^h \delta_{ij}, \quad i, j = 1, 2, \dots, l_h,$$

$$H_{ij}^{22} = \frac{1}{2}(\gamma_1 - \gamma_2)k_{||}^2 \delta_{ij} + \epsilon_j^l \delta_{ij}, \quad i, j = 1, 2, \dots, l_l,$$

$$H_{ij}^{12} = H_{ij}^{21} = (\sqrt{3}/2)\bar{\gamma}k_{||}^2 S_{ij} - \sqrt{3}\gamma_3 k_{||} K_{ij}, \quad i = 1, 2, \dots, l_l, \quad j = 1, 2, \dots, l_h,$$

with

$$S_{ij} = \langle \phi_i^l | \phi_j^h \rangle, \quad K_{ij} = \left\langle \phi_i^l \left| \frac{\partial}{\partial z} \right| \phi_j^h \right\rangle,$$

$$S_{ij} = \begin{cases} B_h B_l \left[\frac{\sin(k_h - k_l)L/2}{k_h - k_l} + \frac{\sin(k_h + k_l)L/2}{k_h + k_l} + \frac{2 \cos(k_h L/2) \cos(k_l L/2)}{\kappa_h + \kappa_l} \right] & \text{for } i, j \text{ both odd,} \\ B_h B_l \left[\frac{\sin(k_h - k_l)L/2}{k_h - k_l} - \frac{\sin(k_h + k_l)L/2}{k_h + k_l} + \frac{2 \sin(k_h L/2) \sin(k_l L/2)}{\kappa_h + \kappa_l} \right] & \text{for } i, j \text{ both even,} \\ 0 & \text{otherwise,} \end{cases}$$

$$K_{ij} = \begin{cases} B_h A_l \left[\frac{k_l \sin(k_h - k_l)L/2}{k_h - k_l} + \frac{k_l \sin(k_h + k_l)L/2}{k_h + k_l} - \frac{2\kappa_l \sin(k_l L/2) \cos(k_h L/2)}{\kappa_l + \kappa_h} \right] & \text{for } i \text{ odd and } j \text{ even,} \\ B_l A_h \left[\frac{k_l \sin(k_h + k_l)L/2}{k_h + k_l} - \frac{k_l \sin(k_h - k_l)L/2}{k_h - k_l} - \frac{2\kappa_l \sin(k_h L/2) \cos(k_l L/2)}{\kappa_l + \kappa_h} \right] & \text{for } i \text{ even and } j \text{ odd,} \\ 0 & \text{for } i, j \text{ even or for } i, j \text{ odd.} \end{cases}$$

Subscripts h or l denote values resulting from heavy- or light-hole masses taken for evaluation of $\epsilon_i, k_i, \kappa_i$, and the normalizing constants A_i, B_i defined in Appendix A. The diagonalization of matrix H , which is in fact the variational Ritz method, provides the eigenenergies and eigenvectors through $a_i(k_{||})$ and $b_i(k_{||})$.

¹See the review paper by R. C. Miller and D. A. Kleinman, *J. Lumin.* **30**, 520 (1985).

²G. Lampel, *Proceedings of 12th International Conference on the Physics of Semiconductors, Stuttgart, 1974*, edited by M. H.

Pilkuhn (Teubner, Stuttgart, 1974), p. 743.

³R. C. Miller, D. A. Kleinman, and A. C. Gossard, *Proceedings of 14th International Conference on the Physics of Semiconductors, Edinburgh, 1978*, edited by B. L. H. Wilson (IOP,

- Bristol, 1978), p. 1043.
- ⁴C. Weisbuch, R. C. Miller, R. Dingle, A. C. Gossard, and W. Wiegman, *Solid State Commun.* **37**, 219 (1981).
- ⁵R. Houdré, Thèse de Doctorat en Physique de l'Université de Paris—Sud, Orsay 1985.
- ⁶W. T. Masselink, Y. L. Sun, R. Fischer, T. J. Drummond, Y. C. Chang, M. V. Klein, and H. Morkoç, *J. Vac. Sci. Technol.* **B 2**, 117 (1984).
- ⁷G. Bastard, *Phys. Rev.* **24**, 5693 (1981); **25**, 7584 (1982).
- ⁸M. Altarelli, U. Ekenberg, and A. Fasolino, *Phys. Rev. B* **32**, 5138 (1985); M. Altarelli, in *Heterojunctions and Semiconductor Superlattices*, edited by G. Allan, G. Bastard, N. Boccarda, M. Lanoo, and M. Voos (Springer, Berlin, 1986), p. 12.
- ⁹We neglect the spin-orbit split band since $\Delta=0.34$ eV in GaAs, and we are dealing here with energies 1 order of magnitude smaller.
- ¹⁰J. M. Luttinger, *Phys. Rev.* **102**, 1030 (1956).
- ¹¹D. A. Broido and L. J. Sham, *Phys. Rev. B* **31**, 888 (1985).
- ¹²A. Baldereschi and N. O. Lipari, *Phys. Rev. B* **8**, 2697 (1973).
- ¹³The subband energies for $k_x, k_y=0$ are determined by the inverse of the bulk light and heavy masses in the z direction, $\gamma_1 \pm 2\gamma_2$, replaced by $\gamma_1 \pm 2\gamma'$ in this approximation.
- ¹⁴*Numerical Data and Functional Relationship in Science and Technology*, Vol. 17 of *Landolt-Börnstein*, edited by O. Madelung (Springer, Berlin, 1982).
- ¹⁵G. Duggan, *J. Vac. Sci. Technol. B* **3**, 1224 (1985).
- ¹⁶R. C. Miller, D. A. Kleinman, and A. C. Gossard, *Phys. Rev. B* **29**, 7085 (1984).
- ¹⁷R. Dingle, in *Festkörperprobleme*, edited by H. J. Queisser (Vieweg, Braunschweig, 1975), Vol. 15, p. 21.
- ¹⁸C. Chang and J. N. Shulman, *Phys. Rev. B* **31**, 2069 (1985).
- ¹⁹T. P. Pearsall, *GaInAsP Alloy Semiconductors* (Wiley, New York, 1982), and references therein.
- ²⁰J. Léotin, R. Barbaste, S. Askenazy, M. S. Skolnik, R. A. Stradling, and J. Tuchendler, *Solid State Commun.* **15**, 693 (1974).
- ²¹P. Rochon and E. Fortin, *Phys. Rev. B* **12**, 5803 (1975).
- ²²C. R. Pidgeon, D. L. Mitchell, and R. N. Brown, *Phys. Rev.* **154**, 737 (1967).
- ²³We only consider excitation to $n=1$ conduction band because excitations to the next subbands are well out of the considered energy range.
- ²⁴G. Lampel, A. N. Titkov, and V. I. Safarov, *Proceedings of the 14th International Conference on the Physics of Semiconductors, Edinburgh, 1978*, edited by B. L. H. Wilson (IOP, Bristol, 1978), p. 1301.
- ²⁵E. F. Gross, A. I. Ekimov, B. S. Razbirin, and V. I. Safarov, *Zh. Eksp. Teor. Fiz. Pis'ma* **14**, 108 (1971) [*JETP Lett.* **14**, 70 (1971)].
- ²⁶U. Fano, *Rev. Mod. Phys.* **29**, 74 (1957); G. Fishman, C. Hermann, and G. Lampel, *J. Phys. (Paris)* **C3-13** (1974); V. D. Dymnikov, M. I. D'yakonov, and N. I. Perel', *Sov. Phys.—JETP* **44**, 1252 (1976) [*Zh. Eksp. Teor. Fiz.* **71**, 2373 (1976)].
- ²⁷M. I. D'yakonov and V. I. Perel', *Zh. Eksp. Teor. Fiz.* **60**, 1954 (1971) [*Sov. Phys.—JETP* **33**, 1053 (1971)].
- ²⁸G. Fishman and C. Hermann, *Phys. Status Solidi B* **63**, 307 (1974).
- ²⁹C. Weisbuch, R. Dingle, A. C. Gossard, and W. Wiegman, *Solid State Commun.* **38**, 709 (1981).